AIAA JOURNAL
Vol. 34, No. 11, November 1996

Large-Eddy Simulations of the Vortex-Pair Breakup in Aircraft Wakes

D. C. Lewellen* and W. S. Lewellen†
West Virginia University, Morgantown, West Virginia 26506-6106

We have utilized large-eddy simulations to simulate the transition from an aircraft wake dominated by the interaction of vortex-pair dynamics and engine plume buoyancy to one dominated by atmospheric dispersion. Our investigation concentrates on the period from a few seconds to several minutes after the wake is generated, during which the essentially two-dimensional vortex-pair is broken up into a variety of three-dimensional eddies. Our initial conditions are taken from near-wake simulations for three aircraft: the B-737, the B-747, and the ER-2. Comparisons of our simulations, for conditions representative of the atmosphere in the upper troposphere and the lower stratosphere, with wake photographs taken from the ground show very similar features. In the absence of wind shear, the vortex pair go through a linking instability that is affected both by engine buoyancy and ambient turbulence. The resultant series of vortex rings continue to descend, leaving the wake with the appearance of a series of suspended puffs. When the mean atmospheric shear is sufficiently large, the ambient vorticity can erode one member of the vortex pair, leading to a breakup mode with a much shorter wavelength.

I. Introduction

THE evolution of aircraft wakes has been an active research subject for more than 25 years.[1] The potential hazards of wake turbulence for following aircraft during takeoffs and landings stimulated much of the early research[2] and remains of primary importance in determining safe following distances at crowded airports. More recently, attention has focused on assessing the impact of increased aircraft traffic on the environment, particularly potential effects of exhaust species on ozone levels in the atmosphere and of persistent contrails on the Earth's radiation balance.[3,4] The dynamics and mixing in the aircraft wake at early times, which we consider in this work, may be expected to ultimately affect the chemical composition of the wake at late times.

It is convenient to identify four overlapping regimes in the evolution of an aircraft wake. During the first few seconds the vorticity distribution from the wing rolls up into a pair of trailing vortices, while the engine exhaust jets mix with the ambient air, largely independent of the roll-up process. The wake dynamics following this roll-up/jet regime are dominated by the interactions of the vortex pair. Typically in this stage the engine exhaust jets partly wrap into the vortex cores and partly detrain into a buoyant plume; the vortices fall and interact with each other through a mutual induction sinusoidal instability and with any ambient shear that is present, until they finally break up, typically within a couple of minutes. After vortex breakup, positive buoyancy acquired from the hot engine exhausts and from the vortex pair falling through any ambient stratification can dominate the dynamics until the plume mixes sufficiently with the ambient air, typically within one or two Brunt–Vaisala periods (~10 min). Finally, at later times, the plume dispersion is dominated by the interaction with the ambient atmosphere, via atmospheric turbulence, gravity waves, and shear.

In the present work we present the results of large-eddy simulations (LES) focused on the middle two regimes of wake evolution, dominated by the vortex interactions and buoyant plume dynamics. We take our initial conditions after roll-up of the wing tip vortices. The configuration and properties of the vortices and exhaust jets prove to be important to the dynamics in our regime of interest, but we take these as given from existing computations. The early stages of vortex interaction have been heavily studied analytically via linear stability analysis[5–9] and numerically in two spatial dimensions,[10–12] including the effects of atmospheric perturbations, stratification, buoyancy, and shear. The sinusoidal linking interaction of the vortex pair is, however, inherently three dimensional and nonlinear, and so these methods are unable to treat the instability through the complete breakup stage. To our knowledge our present work represents the first three-dimensional unsteady explicit simulation of the mutual induction vortex breakup of an aircraft wake. We carry the simulation on through the buoyant plume dominated stage. Since ultimately one of our motivations is to better understand the effects of dynamics and mixing on the chemistry in the aircraft wake, the interaction of the engine exhausts with the vortex breakup plays a larger role in the present work than in most of the existing analyses.

The late time wake dispersion, dominated by the dynamics of the ambient atmosphere, has been the subject of some recent simulations, including some LES.[13–15] (Gerz and Palma[14] simulate the early wake decay as well, for an idealized vortex pair in strong enough ambient turbulence that the vortices disintegrate before they can interact with each other.) For favorable ambient humidity levels the contrail can seed ice formation, and the latent heat released can affect the dynamics at these late stages. We have not included this ice physics in the present simulations as the latent heat effects represent only small perturbations in the vortex and buoyant plume dominated regimes.

It is clear from observations of the evolution of aircraft condensation trails from the ground that there is a large variety of wake decay patterns. Many factors, including the wing and engine configurations, engine heat, atmospheric turbulence, gravity waves, ambient humidity, temperature stratification, and wind shear, affect wake evolution. There are laboratory and aircraft observations,[16–18] but it is difficult to systematically cover much of the parameter space involved. Observations of contrails from the ground are complicated by the possible variations in ambient humidity levels. Typically, if the humidity levels are low enough so that the condensation trails of the vortex pair are easily distinguished, then the contrails evaporate soon after vortex linking; at higher ambient humidity levels the pair are often shrouded together so that the vortex interactions are not seen directly, leaving one to infer the origins of characteristic periodic structures that often appear.

In this work we begin to explore the effects of some of the aircraft and atmospheric variables on the wake decay. Just as in real flight test programs, there is a conflict between costs on one side and coverage of a large parameter space in our LES investigation. A systematic

Received Oct. 26, 1995; revision received June 10, 1996; accepted for publication July 2, 1996; also published in *AIAA Journal on Disc*, Volume 2, Number 1.

*Research Assistant Professor, Mechanical and Aerospace Engineering Department.
†Research Professor, Mechanical and Aerospace Engineering Department. Member AIAA.

treatment varying particular parameters is deferred to future work. Here we isolate and identify some characteristic features of the wake decay and correlate them with features such as the periodic series of puffs that are generically observed in contrail evolution (and have been the subject of speculation in the literature[19]).

In Sec. II we review our LES model and the modifications required for the contrail problem. In Sec. III we describe the initial conditions used and the logistics for a simulation. In Sec. IV we present results from four large-eddy simulations: a Boeing 737, a Boeing 747 with and without wind shear, and the ER-2 in the stratosphere. These are used to illustrate some of the qualitative features found generically in aircraft wake decays. Finally, in Sec. V we give some concluding remarks.

II. Model Review

The Reynolds numbers for atmospheric flow problems are sufficiently large that direct numerical simulations of the Navier–Stokes equations are not possible with current (or immediately foreseeable) computational resources. Large-eddy simulations attempt the next best solution, resolving the most important eddies and relying on turbulence modeling only for subgrid scale eddies, which are (we hope) of secondary importance. For this work we modified an LES code developed primarily for boundary-layer cloud modeling.[20,21] This is a three-dimensional finite difference implementation of the incompressible Navier–Stokes equations in the Boussinesq approximation, second-order accurate in space and time. The subgrid model utilizes a quasi-equilibrium, second-order turbulence closure scheme with the maximum subgrid turbulence length scale related to the numerical grid length. Recent versions of the code[22,23] incorporate a piecewise parabolic model algorithm for the advection of temperature and species concentrations. This proved quite beneficial for the current application in minimizing numerical diffusion of sharp concentration gradients occurring, for example, as the engine exhausts wrap around the vortex cores.

Efficiently modeling an aircraft wake's evolution necessitated a number of modifications to the basic LES code. The principal difficulty in this problem is one of resolution. A grid spacing of a few percent of the wing span or less is required to resolve the trailing vortex cores and the transport of the engine exhausts around and into them. On the other hand, line vortices have a sizable long-range influence on the flowfield, so that domain widths of several wingspans or more are required to minimize unwanted boundary interactions. To best meet these conflicting demands we modified the LES code to allow for a grid stretched independently in all three dimensions. In the region of the domain occupied by the vortices the grid is fine and uniform; in the region that will contain the spreading wake the grid is coarser, with a degree of stretching of 10% or less between neighboring grid points allowed. Far from the wake near the domain boundaries the grid spacing is typically a factor of 15–20 times larger than the finest spacing. We employ a direct solver for the Poisson equation for the pressure, which is used to impose the incompressibility condition, on this stretched grid.[24] This is computationally less efficient than fast Fourier transform methods, which can be applied on a uniform grid, but allows us to employ an order of magnitude fewer grid points (typically ~750,000) than a uniform grid would require for the same resolution in the immediate vortex region given the same domain size.

The grid was moved at a constant velocity with respect to the ambient atmosphere to keep the falling vortex pair within the fine grid region of the domain. This grid translation velocity was adjusted at a few discrete times during the simulations when necessary to account for changes in the pair fall velocity and, later, for the buoyant rise of the wake. The calculations were at all times performed in an inertial frame of reference. As the wake evolves, its vertical and horizontal extent increases; at the same time the vortices are breaking up and diffusing. In time, then, less resolution is required to simulate the wake dynamics, but with the finer resolution portion extending over a larger domain. To account for this we interpolated the species and flowfields to new stretched grids when it appeared beneficial during a simulation. In some cases, we increased the domain volume as well. In the four simulations presented in the next section, two to four grids were employed in each case. In several cases segments of the simulations were run both with the old and new grids and the results compared to confirm that the coarser grid was still sufficient to resolve the most important dynamics.

We employ periodic boundary conditions in all three directions. Effectively this means there are neighboring wakes located at twice the distance to the boundary in the vertical and crosswise directions evolving in parallel with our simulated wake. The stretched grid allows us to place the boundaries at sufficient distance to minimize boundary effects.

In treating the wake decay we made only one modification to the basic equations solved by the LES code. We extended the Boussinesq approximation to include centrifugal buoyancy effects, thereby including the tendency for the warm jet exhausts to be pulled into the low-pressure vortex cores. This effect was incorporated by including the product of the potential temperature perturbation times the pressure gradient, in the same spirit as the gravitational buoyancy term is included. In our simulations this effect proved to be of little importance, however.

III. Initial Conditions

Under cruise conditions a jet aircraft flies fast enough that the age difference between the beginning and end of a modest length segment of the aircraft wake is small compared with the time scales relevant to the wake's subsequent evolution. This permits us to take a uniform length of wake (with periodic boundary conditions) as our initial flowfield to a good level of approximation. For our initial wake cross sections we use output from the UNIWAKE program.[25] This utilizes a modified Betz methodology for the roll-up of the vortex sheet followed by a two-dimensional parabolic marching calculation for the early wake evolution. We take the three velocity components, temperature, and turbulent kinetic energy from these results and add a tracer species concentration with the same distribution as the temperature and an arbitrary normalization. Thirty percent of the turbulent kinetic energy is converted into grid scale random perturbations of the velocity fields to initialize some small scale three-dimensional turbulence in our simulations. We typically use the UNIWAKE results of order 20 wingspans behind the aircraft (a few seconds). This is late enough so that the roll-up is essentially complete and the exhaust jets have grown enough (through entrainment of ambient air) to be more easily resolved, but early enough so that the important wake dynamics are still two dimensional. Picking the wake up this early allows us to include some effects (e.g., atmospheric stratification) not present in the UNIWAKE simulation and provides time for three-dimensional perturbations to grow before the dynamics becomes predominantly three dimensional.

In this work we present the results from four simulations. Table 1 summarizes some aircraft, atmospheric, and numerical parameters for these simulations. The initial vortex separation b_0, core radius, circulation Γ, and initial fall time t_f (defined as the initial vortex separation divided by the initial pair fall velocity) are approximate numbers taken from the UNIWAKE flowfield used to initiate the simulation. They give some indication of the nature of the initial flowfields and differences between different aircraft. Similarly, the cross-sectional integration of the temperature excess in the exhaust jet, $\int \Delta T \, dy \, dz$, gives an indication of the relative importance of engine heat in each simulation. The two-dimensional domains used for the UNIWAKE computations were smaller than our cross-stream domains. We assumed Gaussian vorticity distributions (using the circulations and core radii in Table 1) for the purpose of extending the UNIWAKE fields beyond the central region and to include the contributions from the periodic image wakes (to make our initial fields periodic). The Gaussian fit need not be perfect because it is only used for the far field and because a field of ambient turbulence and waves (to be discussed later) is also superimposed on this field. The conditions used for the B-747 UNIWAKE simulations are somewhat less representative of actual cruise conditions than those given for the B-737 and ER-2, as they were scaled from some low-altitude flyby tests.

The minimum grid spacings listed in Table 1 (downstream × cross stream × vertical) are those used for the initial time segment of each simulation in the portion of the domain occupied by the wake. The smallest grid spacing is required in each of the cross-stream directions. Comparison with the higher resolution UNIWAKE results and our own higher resolution tests (run with short downstream domains)

Table 1 Initial simulation conditions

Simulation	1	2	3	4
Aircraft	B-737	ER-2	B-747	B-747
Span, m	28.9	31.4	60.8	60.8
Airspeed, m/s	244	201	268	268
Engines	2 wing	1 tail	4 wing	4 wing
$\int \Delta T\, dy\, dz$, Km^2	1.1×10^3	4.3×10^2	8.6×10^3	8.6×10^3
Vortex sep., m	22.7	23.9	47.4	47.4
Core radius, m	2.5	5.0	4.6	4.6
Circulation, m^2/s	220	383	414	414
t_f, s	14.7	9.4	34.1	34.1
Atmospheric				
N, s^{-1}	0.012	0.021	0.012	0.012
Shear S, s^{-1}	0	0	0	0.02
TKE, m^2/s^2	0.1	0.05	0.09	0.07
Numerical				
Domain, km	$0.2 \times 0.24 \times 0.32$	$0.2 \times 0.24 \times 0.32$	$0.4 \times 1 \times 1$	$0.2 \times 1 \times 0.8$
Min. grid, m	$2 \times 1 \times 1$	$2 \times 1.1 \times 1.1$	$4 \times 2 \times 2$	$2 \times 2 \times 2$

indicated that the grid spacings in Table 1 were sufficient to resolve the circulation of the engine exhausts about the vortex cores.

The initial vertical and cross-stream domain lengths given in Table 1 were chosen large enough so that boundary effects are minimal. The minimum dimensions are at least 10 vortex separation lengths; i.e., the closest periodic image pairs are more than 10 vortex separations away. The velocity field produced by a pair of oppositely circulating line vortices falls at long distances as $\Gamma b_0/2\pi D^2$, where D is the distance to the pair. Summing the contributions from all of the periodic images in the cross-stream direction, for example, would contribute $\pi\Gamma b_0/(6D^2)$ to the vertical velocity field in the center of our domain, which in our simulations amounts to less than a 5% change in the resulting pair fall velocity. The resultant change in velocity gradients across the wake amounts to less than a 1% perturbation. Later in the wake evolution, after the vortices break up, these effects become unimportant, but the vertical and cross-stream dimensions of the wake itself increase; the domain must remain large enough to avoid any appreciable interactions with the boundaries. Accordingly, the domain dimensions were increased for the late time portions of some of the simulations: the vertical dimensions to 500 m in simulations 1 and 2 and 900 m in simulation 4 and the cross-stream dimension to 600 m in simulation 1 and 1600 m in simulation 4.

The downstream domain lengths for our simulations were chosen on the basis of quite different considerations. We know from observations, previous analyses, and our own simulations that the principal vortex breakup mode (for low-to-moderate atmospheric turbulence and shear) is a relatively long wavelength sinusoidal instability. The choice of a downstream domain length necessarily constrains the wavelengths available for this instability because an integral number must fit into the domain. In his original analysis, Crow[5] found the wavelength of the maximally amplified unstable mode to be $8.6b$; later work showed a modest dependence of this quantity on the vortex core radius and axial velocity.[6] The amplification rate is not, however, a sharply peaked function of wavelength; perturbations over a broad range of wavelengths grow almost equally fast.[9] Thus the actual wavelength that will be observed for the vortex pair instability will largely be determined by the wavelengths of the strongest perturbations present initially. In the atmosphere a broad range of possibilities may occur; here we just want some representative realizations, and so we have taken the downstream domain lengths to be on the order of the Crow value for the initial vortex spacing (Table 1). The exception is simulation 4, the B-747 with shear. There were two reasons for the shorter domain choice in this case. First, we found in the B-747 simulations, as will be discussed in the following section, that the vortex-pair spacing decreases in time and the instability correspondingly tends to grow on shorter wavelengths. Second, in the presence of large shear, the sinusoidal instability does not progress to completion and shorter wavelength rotational instabilities play a larger role in the vortex breakup.

To complete the initial fields for our simulations we superposed the initial aircraft wake fields onto an ambient atmospheric field. For simulations 1, 3, and 4 we chose a potential temperature gradient (3×10^{-3} K/m) appropriate for the troposphere and for simulation 2 a value (0.01 K/m) appropriate for the stratosphere corresponding to the Brunt–Vaisala frequencies N listed in the table. Simulation 4 includes a sizable level of vertical wind shear. The periodic boundary conditions in the vertical dimensions were implemented with a jump in temperature, and in velocity for case 4, to be consistent with the ambient stratification and shear.

Each initial background field included some atmospheric turbulence and gravity waves. Table 1 lists the initial levels of the turbulent kinetic energy (TKE) in the domain volume for the background fields used for each simulation. These turbulence levels are small compared with the initial circulations in the wake vortices. Their major role is to serve as sources for perturbations (over a range of wavelengths) to allow the sinusoidal vortex-pair instabilities to develop. The perturbations on actual aircraft wakes may arise from a number of sources. These include atmospheric turbulence, gravity waves, and unsteady wing loading (giving variations in vortex circulation) and, for quiescent atmospheres, rotational turbulence on the vortices, exhaust jet turbulence, and the wrapping of the exhaust jets around the vortices. (The wavelength for the last source is fixed by the vortex circulation and distance to the engine and so is potentially important only for some aircraft.) The precise source of perturbations is not of particular importance for the subsequent vortex breakup—only the wavelength and magnitude. Furthermore the dependence on the actual magnitude is not too strong as demonstrated by Bliss.[9] Since the instabilities grow exponentially, the time required for the sinusoidal perturbations to grow to a certain level depends only logarithmically on the magnitude of the initial perturbations. This is not to say that the level of the atmospheric perturbations are unimportant. They will directly determine that the time linking will occur. In this work we seek to simulate a few representative realizations of vortex breakup and so don't attempt to span the broad range of actual possibilities. Thus it suffices to employ background atmospheric fields with turbulence levels and spectra within what is a broad range of reasonable physically occurring possibilities.

We generate the background fields as follows. We begin with the domain dimensions and temperature stratification to be used for the wake decay simulation. On a uniform coarse grid (10–20 m spacing) we generate random horizontal velocity and temperature perturbations of relatively large magnitude. These are interpolated to a finer grid (5–10 m spacing) and used as initial conditions in a large-eddy simulation. This simulation is run until the turbulence and gravity waves have a chance to adjust to the temperature stratification and have damped to the desired amplitude range (Table 1). When the initial aircraft wake is superimposed on this field, it provides modest random perturbations on a variety of wavelengths commensurate with the periodic domain. This is sufficient for the simulation periods considered here; however, for longer simulations, after the vortex breakup and buoyant plume dynamics have subsided, the atmospheric turbulence will begin to dominate the dynamics. For this regime our background fields with decaying atmospheric turbulence

are not typical of real conditions and some driving mechanism to sustain the turbulence will be desirable.

IV. Simulation Results and Comparison with Observations

Figure 1 shows a typical aircraft wake as exhibited by its condensation trail photographed from the ground a few minutes after the passage of the aircraft. Neither the aircraft type nor the atmospheric conditions are known, but, as our simulation results will illustrate, the qualitative features observed occur for a variety of aircraft and atmospheric conditions. The clear periodicity observed in such wakes provides support for the validity of employing short downstream domains with periodic boundary conditions in our simulations. In each of the simulations presented here the computational domain encompasses only one or two periods of the basic decay mode. This is sufficient for a qualitative understanding of the basic underlying wake decay dynamics and its dependence on some aircraft properties and atmospheric conditions, and serves as a first quantitative estimate of these effects. A statistically accurate ensemble average of the wake evolution, however, would require averaging over either a much longer downstream domain or several small domain simulations (with small variations in initial perturbations and domain sizes) to include the period to period variations seen in Fig. 1. The downstream averages presented later should be considered only a first approximation to the true ensemble average. Variations from left-right symmetry provide some indication of the departures from an ensemble average.

In the time sequences illustrated in Figs. 2–5, we pick up the B-737 wake decay at about the time that three-dimensional effects become important, these being our main subject of interest. Before this stage, in the early wake, the warm engine exhausts wrap around the vortices with some fraction captured within the vortex cores and some positively buoyant fraction detrained into an exhaust wake lying above the vortex pair. Simultaneously, the vortex pair falls with approximate velocity $\Gamma/2\pi b$, and initial long wave perturbations on the vortices grow via interaction between the mutual and self-induced velocity fields from the vortices. The vortex-pair separation b and fall time, $t_f = 2\pi b^2/\Gamma$, provide the basic length and time scales relevant to the growth of these perturbations. The details of how the engine exhausts wrap into the vortices are important but are not the main thrust of this paper.

Figure 2 shows the downstream average of the tracer concentration C, which is representative of conserved, passive releases from the engines. The distribution is shown at five successive times for the B-737 wake simulation. In this plot and the other corresponding figures, the spacing between tick marks on the frame perimeters represent 25 m to indicate the scale, and the contoured variable has been scaled in some frames (as noted in the figure captions) to allow a single label bar to be used for each figure. Figure 2a shows this approximate ensemble average at a dimensionless fall time of 2.0. The maximum tracer concentration is in the core of

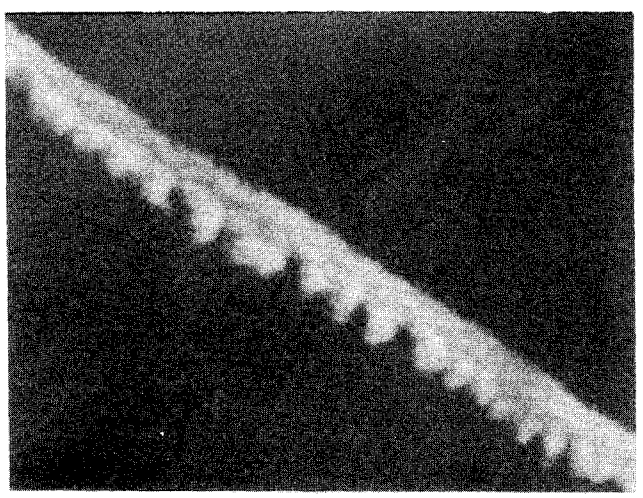

Fig. 1 Photograph of an aircraft contrail aged approximately 3 min.

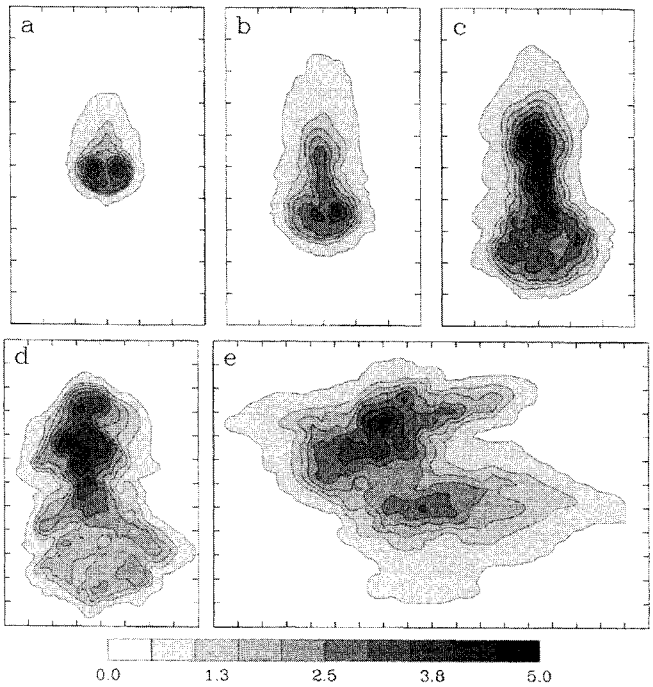

Fig. 2 Downstream average of the tracer concentration for the B-737 wake, simulation 1: a) C at 30 s, b) $2C$ at 60 s, c) $5C$ at 93 s, d) $10C$ at 188 s, and e) $15C$ at 599 s.

the vortices, with relatively little detrained from the ellipse moving down with the vortex pair. Later figures will show that there is three-dimensional structure at this time, but it is sufficiently small that a two-dimensional description of the wake at this point is not unreasonable. Figure 3 shows the corresponding cross-stream integrated tracer fields, normalized by the wingspan b_s, i.e., $\int C\,\mathrm{d}z/b_s$. The peak value of this tracer field at the beginning of the simulation is normalized (arbitrarily) to be 100. This two-dimensional projection of the field gives some approximation of how the decaying wake might appear to the eye as viewed from the side. For clarity we have included some of the periodic domain images downstream. It shows some early clumping along the wake on a scale of approximately one vortex separation, but this gives way to the longer instability by Fig. 3b, which shows the projection at 4.1 fall times.

Figures 4 and 5 show two-dimensional projections (top and side, respectively) of the dynamic pressure field at selected times, normalized by the density times the span $[-\int P\,\mathrm{d}z/(\rho b_s)$ and $-\int P\,\mathrm{d}y/(\rho b_s)$, respectively] to give units of meters squared per second squared. These clearly show the low-pressure regions in the vortex cores and so give some information on the interior dynamic structure of the wake that is masked in the two-dimensional projections of Figs. 2 and 3. By on order of one fall time in this B-737 wake simulation (i.e., just before the initial frame in Fig. 4) the vortex pair is perturbed sufficiently that a two-dimensional description is beginning to become inadequate to capture the subsequent dynamic evolution.

The growth of unstable modes progresses until the vortex cores touch each other, interact, and link off to form vortex rings (Fig. 4). As seen in Figs. 4 and 5, unstable modes of different wavelengths compete with one another. At 20 s there are strong perturbations at wavelengths on order of 50, 100, and 200 m. At 40–60 s the 200-m perturbation has linked off, but a strong mode of half that wavelength remains, so that the ring nearly splits into two; however, the downward curvature of the ends of the vortex ring (evidenced in Fig. 5c at 60 s) induces an outward velocity in the middle of the ring, forcing the approaching edges back apart. The single ring remains, oscillates under the influence of the velocity field induced by the ring curvature, and finally dissolves some time after 2.5 min. The ring formation and oscillations are qualitatively similar to those observed in aircraft wakes (e.g., photographs in Ref. 2). The ring oscillations observed also agree qualitatively with the numerical and experimental studies of elongated vortex rings by Dhanak and deBernardinis[26];

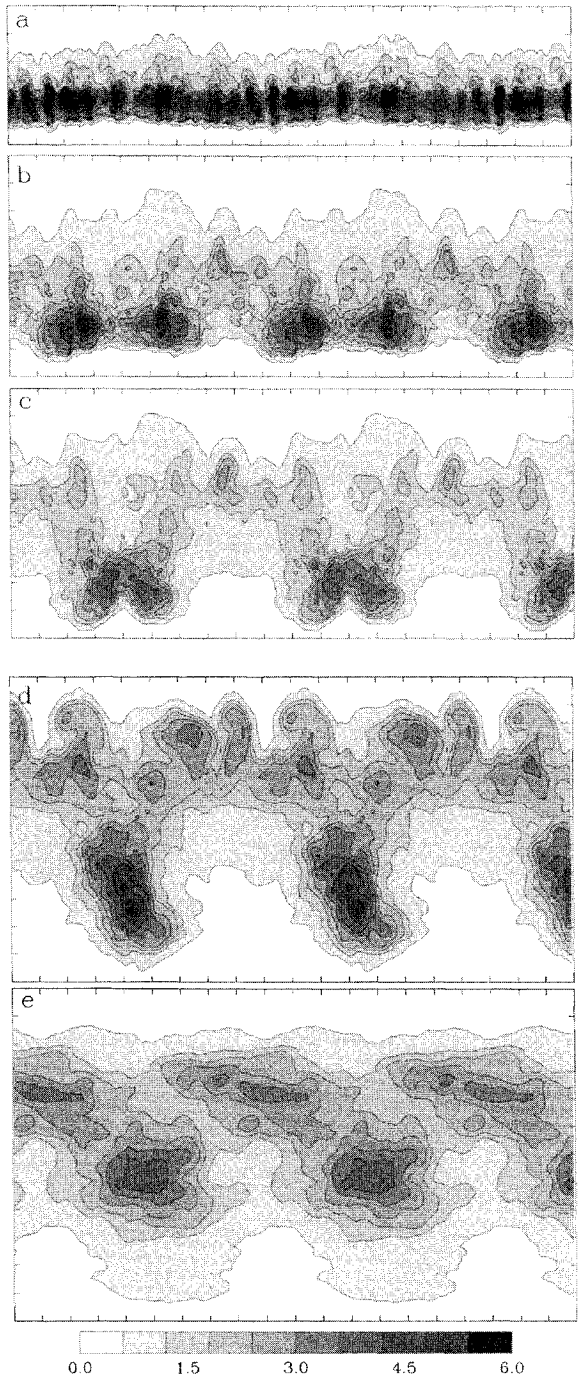

Fig. 3 Cross-stream projection of the tracer concentration $C_y = \int C\,dy/b_s$ for simulation 1: a) C_y at 30 s, b) C_y at 60 s, c) C_y at 93 s, d) $2C_y$ at 188 s, and e) $2C_y$ at 599 s.

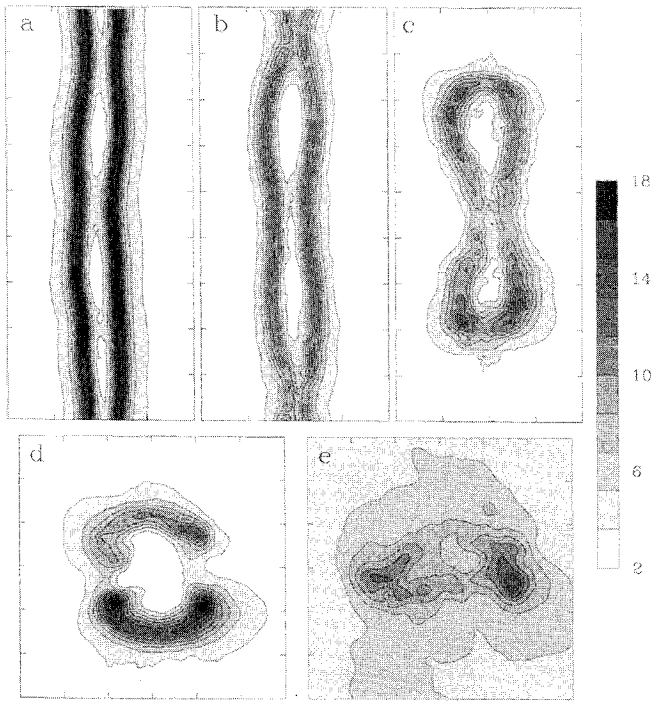

Fig. 4 Vertical projection of the pressure deficit, $P^* = -\int P\,dz/(\rho b_s)$ (in meters squared per second squared), caused by the vortices for the B-737 wake, simulation 1: a) P^* at 20 s, b) P^* at 40 s, c) $2P^*$ at 60 s, d) $4P^*$ at 98 s, and e) $8P^*$ at 148 s.

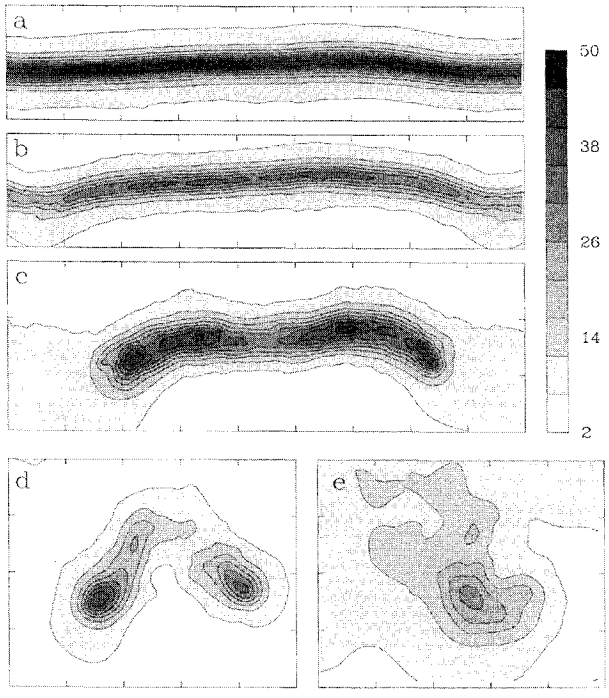

Fig. 5 Cross-stream projection of the pressure deficit, $P_y^* = -\int P\,dy/(\rho b_s)$, caused by the vortices for the B-737 wake, simulation 1: a) P_y^* at 20 s, b) P_y^* at 40 s, c) $3P_y^*$ at 60 s, d) $4P_y^*$ at 98 s, and e) $10P_y^*$ at 148 s.

the absence of initial downward ring curvature and stratification in their studies prevents a more quantitative comparison.

In Figs. 2 and 3 we can follow the vertical spreading of the engine exhaust tracer concentration during the vortex linking, ring, and breakup stages. In Fig. 2 the individual frames are aligned vertically with each other. It is apparent, then, that the increasing vertical extent of the wake arises primarily from the falling vortex pair (and later rings) with a relatively more modest contribution from the rise of the positively buoyant detrained exhaust plume wake. It is the falling vortex rings that are directly responsible for the periodic series of descending puffs often observed in contrail evolution (e.g., Fig. 1). Variations in linking wavelength and ring oscillations lead to the variations observed between different puffs. This description differs from that given by Scorer and Davenport.[19] In explaining the appearance of structures such as those in Fig. 1, they also attribute the upper part of the contrail to fluid detrained from the falling vortex pair but associate the descending puffs with the linking points of the pair rather than the rings (i.e., a description of the puffs half a period out of phase with that given here).

Note that in our results the engine tracer distributions do not in general provide a reliable signature for the underlying vortex dynamics. In the early wake small axial velocity variations, and variations in the exhaust capture vs detrainment, lead to pronounced downstream

fluctuations of tracer concentration in the vortex cores (e.g., Fig. 3a), whereas the vortices themselves remain quite uniform downstream (e.g., Figs. 4a and 5a). This may explain the frequent observation in experiments of vortex bursting (sometimes attributed to vortex breakdown), which is, however, unaccompanied by any significant change in the vortex interactions or dynamics.[16–18] In addition, we find in our experiments that the highest tracer concentration tends to become scrambled and no longer coincides with the center of the vortex cores after linking takes place. This apparent dissolution of the tracer concentration signature for the vortices is clearly not a reliable indication that the vortices themselves have broken up, as is often assumed.

When the vortex rings have finally dissolved, the wake has reached its maximum vertical extent in our simulations (e.g., Figs. 2d and 3d at a dimensionless fall time of 12.8), and buoyant forces proceed to dominate the dynamics. The remnants of the vortex rings are positively buoyant and begin to rise, whereas the top of the wake rises at a slower rate, eventually overshoots its equilibrium point, and begins to fall. In our B-737 simulation there is no vertical shear so the wake collapses onto itself (cf. Fig. 3e). In the atmosphere there will generally be at least a small level of vertical shear, which is sufficient to horizontally displace the top and bottom of the wake. During a buoyant oscillation of the plume the remnant ring puffs will then appear first below, then to the side, then on some occasions above the remainder of the wake plume. The characteristic time scale for these oscillations is a Brunt–Vaisala period $2\pi/N$, set by the vertical temperature stratification (cf. Table 1).

The general features described in the B-737 wake simulation appear as well in the three other simulations listed in Table 1, and so in presenting these latter results we will concentrate on a few characteristic differences between the simulations and their origins. Figures 6–13 show the two-dimensional integrated tracer concentrations and dynamic pressures for simulations 2–4 at different times. Figure 13 represents a vertical integration of the field, which is more informative than the cross-stream integration for the sheared wake.

The positions of the engines with respect to the wing tips can have a significant influence on the development and appearance of the wake. Our second simulation is for the wake of the ER-2. The exhaust from the single tail engine has a more difficult time getting wrapped into the core of the trailing vortices. As seen in Fig. 6, the maximum concentration at any point in time remains outside the vortex cores. This results in a strong, well-defined, detrained exhaust wake above the vortex pair, though the descending vortex rings still capture appreciable tracer (Figs. 6 and 7). Such detrained

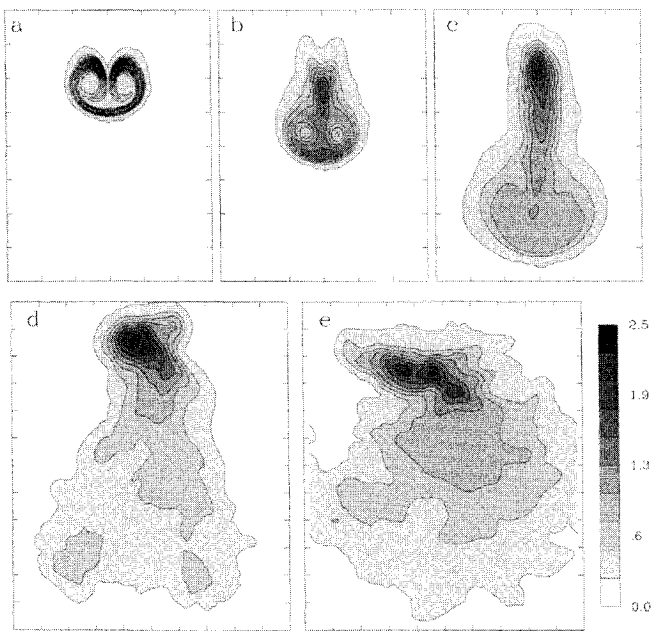

Fig. 6 Downstream average of the tracer concentration for the ER-2 wake, simulation 2: a) C at 15 s, b) $2C$ at 30 s, c) $4C$ at 62 s, d) $8C$ at 146 s, and e) $12C$ at 325 s.

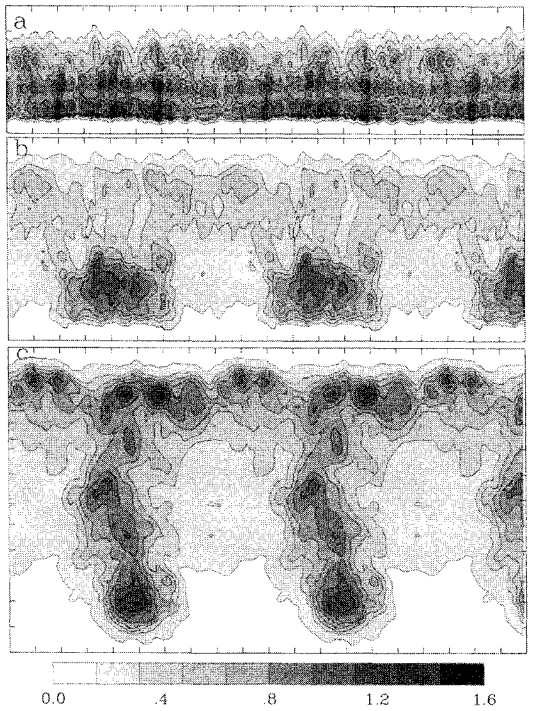

Fig. 7 Cross-stream projection of the tracer concentration for simulation 2: a) C_y at 30 s, b) C_y at 62 s, and c) $2C_y$ at 146 s.

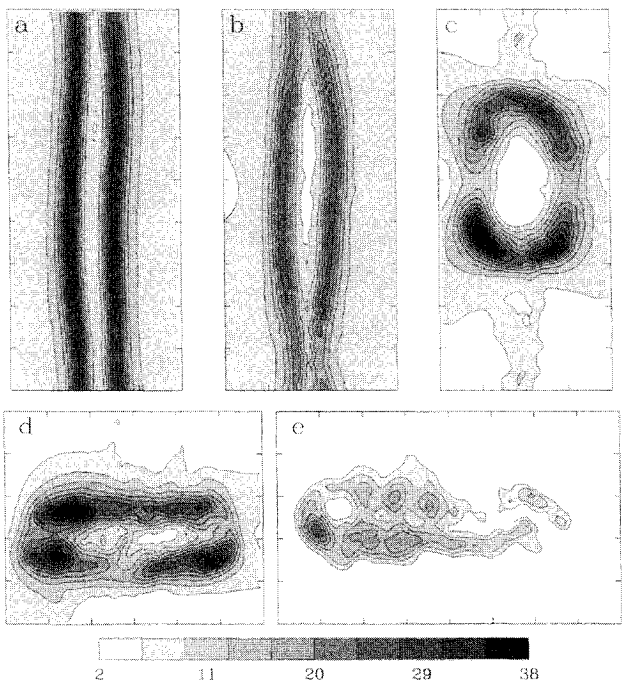

Fig. 8 Vertical projection of the pressure deficit, for simulation 2: a) P^* at 20 s, b) P^* at 40 s, c) $2P^*$ at 62 s, d) $4P^*$ at 87 s, and e) $12P^*$ at 122 s.

exhaust wakes can easily be mistaken for one member of the vortex pair when viewed from the ground since the vortex pair themselves are often enshrouded within a single cloud. The vortex linking takes place at a somewhat faster pace in this simulation compared with the B-737, consistent with the smaller t_f. In this particular simulation the longer wave perturbation happened to easily dominate the lesser components. A fairly symmetrical ring formed and proceeded to oscillate. Initially stretched in the downstream direction, it became nearly circular by 60 s (Fig. 8c), and stretched then in the cross-stream direction (Figs. 6d and 8d) before dissolving. Evidence for such configurations can be seen from the ground under appropriate

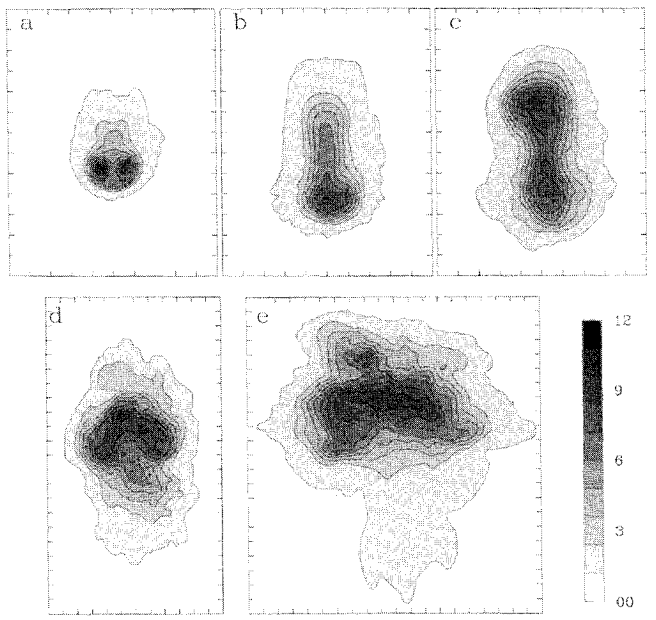

Fig. 9 Downstream average of the tracer concentration for the B-747 wake, simulation 3: a) C at 32 s, b) $2C$ at 62 s, c) $4C$ at 92 s, d) $8C$ at 182 s, and e) $16C$ at 362 s.

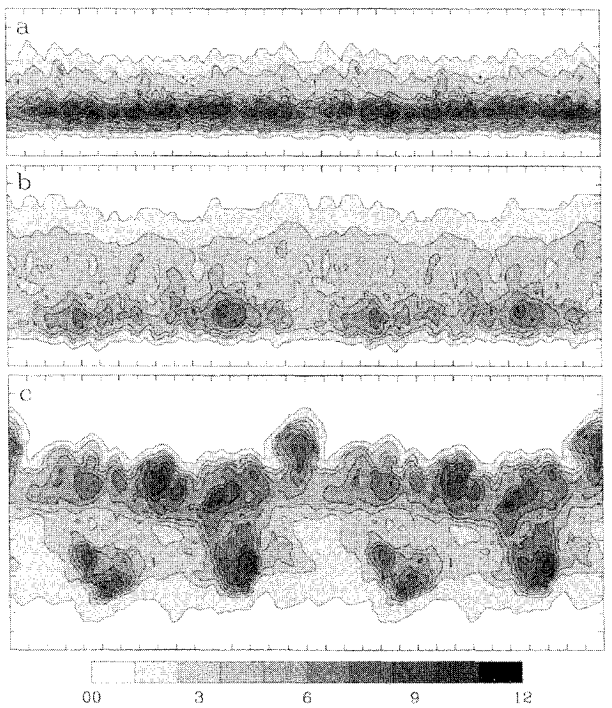

Fig. 10 Cross-stream projection of the tracer concentration for simulation 3: a) C_y at 32 s, b) C_y at 62 s, and c) $2C_y$ at 122 s.

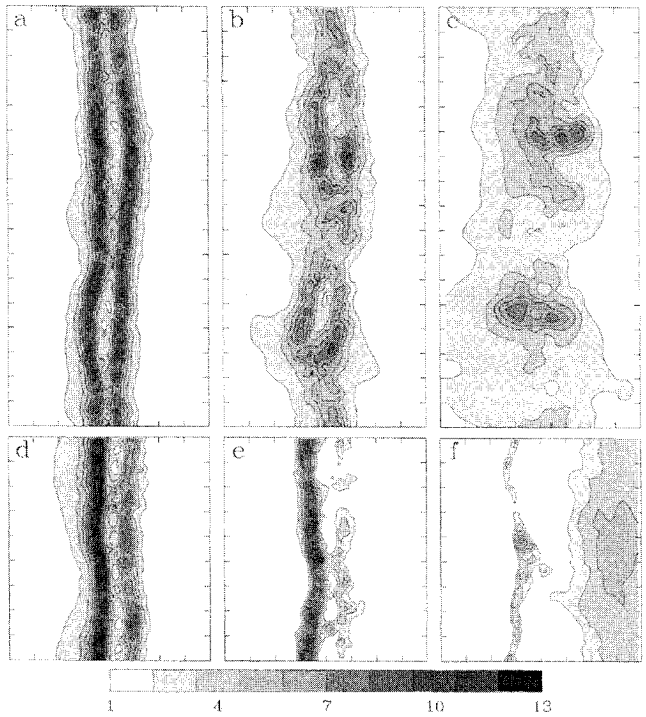

Fig. 11 Vertical pressure projection for B-747 wake without and with shear, simulations 3 (a–c) and 4 (d–f), respectively: a) and d) P^* at 42 s, b) and e) $2P^*$ at 62 s, and c) and f) $3P^*$ at 82 s.

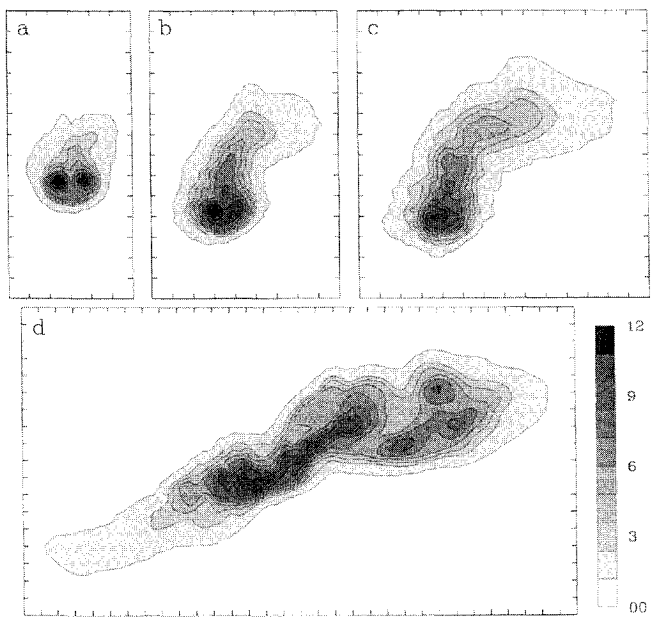

Fig. 12 Downstream average of the tracer concentration for the B-747 wake with wind shear, simulation 4: a) C at 32 s, b) $2C$ at 62 s, c) $3C$ at 92 s, and d) $12C$ at 212 s.

conditions with an aircraft flying directly overhead—the puffs form nearly symmetrically on either side of the remaining wake trace. The shorter Brunt–Vaisala period characteristic of the stratosphere is seen in the earlier collapse of the wake (Fig. 6e) relative to the B-737 simulation.

In the B-747 simulations (3 and 4 in Table 1) the buoyant forces on the hot engine exhausts played an important dynamical role in the wake decay. The exhausts from the four wing-mounted jets (particularly the two outboard) are easily rolled into the vortex cores (as seen in Fig. 9). The added heat from the engines makes the vortex cores positively buoyant relative to their immediate surroundings. The vertical force induces a horizontal velocity that then decreases the vortex pair separation.[27] This speeds up the vortex descent, reduces the effective fall time, and decreases the observed wavelength for the linking instability. The observed evolution thus proceeds on length and time scales close to those found in the B-737 simulation despite the near factor of 2 increase in the initial b and t_f listed in Table 1. In our simulations, this buoyant force on the vortex cores had a much larger impact than the buoyant force on the pair as a whole arising from the stratification of the ambient atmosphere, an effect that has been considered more in the literature. In our simulations this latter effect was found to increase the pair separation slightly over time, when the heat from the engines was not included.

The fourth simulation is a repeat of the 747 wake with only the mean wind shear changed. The shear S chosen corresponds to a

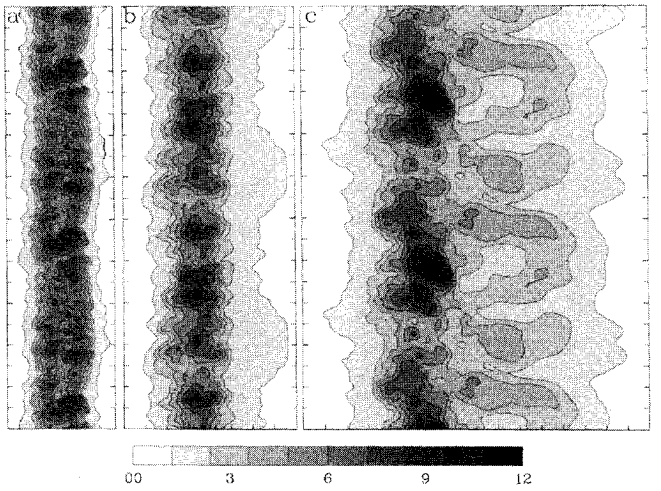

Fig. 13 Vertical projection of the tracer concentration $C_z = \int C\, dz/b_s$ for simulation 4: a) C_z at 32 s, b) C_z at 62 s, and c) $2C_z$ at 122 s.

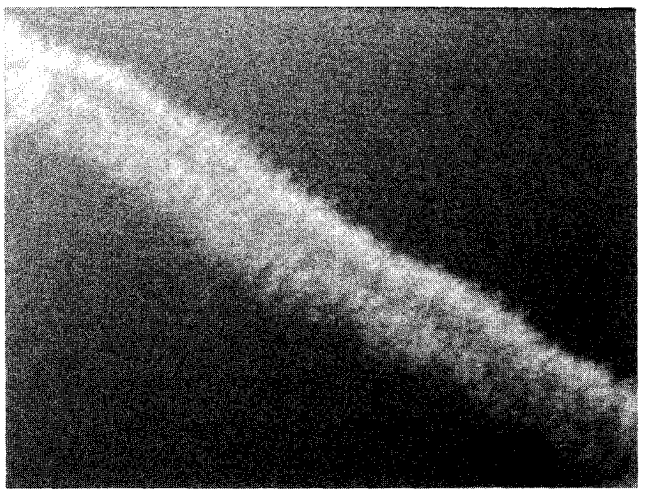

Fig. 14 Photograph of sheared wake.

Richardson number (N^2/S^2) equal to 0.36, which remains stable. The influence of the shear on the downstream average is evident as early as 30 s into the wake lifetime (Fig. 12a), where a slight asymmetry in the vortex pair may be seen. The ambient mean vorticity tends to amplify the vortex on the left, while eroding that on the right. The buoyant force on the vortex cores together with the shear gives rise to the tilting of the vortex pair, just evident in Fig. 12a. The early wake evolution is otherwise similar to the 747 without shear, with the vortex pair instability growing on similar length and time scales. Before the vortex cores draw close enough to touch, however, the rightmost vortex is sufficiently eroded that no linking takes place (Figs. 11d–11f). The remaining deformed vortex breaks up on shorter wavelengths via rotational instabilities and interaction with remnants of the eroded vortex. In this simulation the time scales for the growth of the pair instability and for the erosion of one vortex interacting with the shear (t_f and 1/shear, respectively) were comparable. Clearly, in varying the shear, a continuum of possibilities exists, from low shear levels where the pair instability runs to completion, to high levels in which one member of the vortex pair is quickly eroded by the shear before the mutual induction instabilities have any time to grow. A photograph of a real sheared wake qualitatively resembling Fig. 13 is given in Fig. 14. Again the details of the aircraft and atmospheric conditions in this photograph are unknown.

Figures 15–17 give rough quantitative measurements of the time development in the four simulations. In Fig. 15 the peak tracer concentration in the three-dimensional field is plotted vs time. At the beginning of each simulation this value was arbitrarily set at 100.

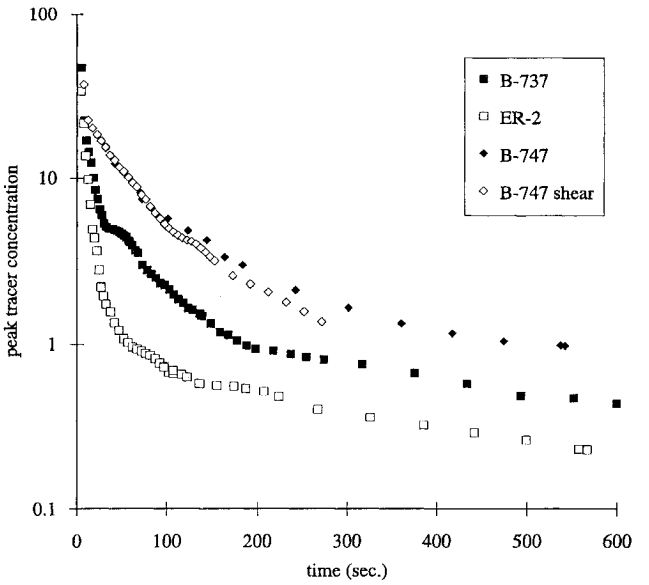

Fig. 15 Maximum tracer concentration in the computational domain as a function of time for all four simulations.

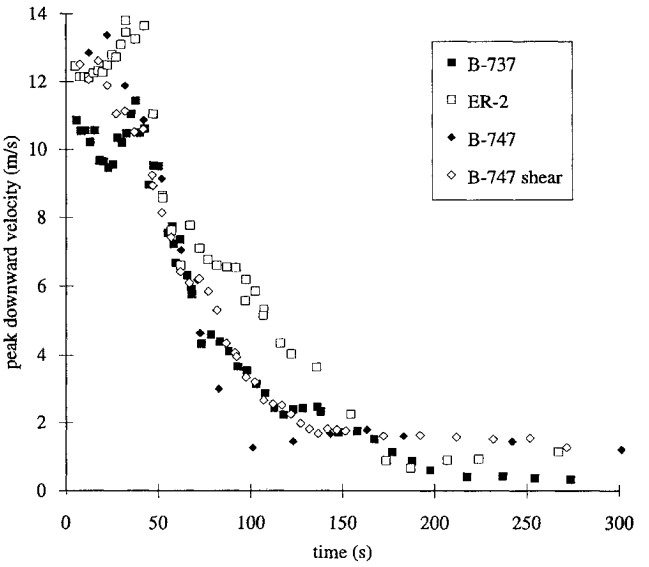

Fig. 16 Maximum downward vertical velocity in each simulation vs time.

The biggest difference between the simulations depends on whether the tracer has been effectively wrapped into the vortex cores or not. The maximum concentration decays the slowest for the two 747 cases where the tracer was very effectively wrapped into the vortex core, whereas that for the ER-2, for which very little of the tracer reached the core, decays the fastest. In the former cases the peak concentration is associated with the vortices and their remnants after breakup; in the latter case it is associated with the detrained exhaust plume above the vortices. In the B-737 simulation the peak concentrations are found in the vortex cores for the first 2 min and in the upper wake plume later on.

Figure 16 shows the magnitude of the maximum downward vertical velocity in the domain (which is found between the vortices at the inner edge of the vortex cores before breakup) vs time. There is a little acceleration in this velocity as a result of stretching of the vortices just before the steepest drops occur during the linking stage (at around 50 and 40 s, respectively, for the B-737 and ER-2). Figure 17 plots the time history of the vertical extent of the exhaust tracer plume as determined from the two-dimensional downstream average field using a contour of 10% of the maximum downstream average concentration to define the edges of the wake plume. The

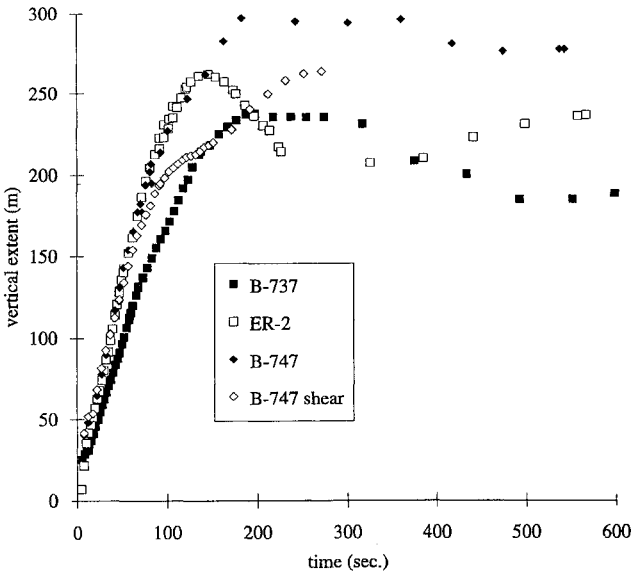

Fig. 17 Vertical extent of the wake plume vs time for each simulation.

rapid growth of the vertical extent at early times in the simulations coincides with the lifetime of the falling vortex pair (and later rings). The characteristic Brunt–Vaisala oscillations can be seen at later times.

V. Concluding Remarks

Our model results of trailing vortices interacting with engine buoyancy and typical atmospheric values of stability, wind shear, and ambient turbulence form a consistent view of vortex breakup, which is in qualitative agreement with photographs taken from the ground. The simulations allow us to study, in detail, dynamics that are primarily hidden within the condensation trail when viewed from the ground. A two-dimensional representation of the aircraft wake is not generally valid past approximately one to two characteristic fall times. In the absence of high wind shear levels, the vortex pair interact and link through a mutual induction instability. The resultant series of vortex rings continue to descend until they break up, leaving the wake with the appearance of a series of suspended puffs. The vertical extent of the wake plume is largely determined by the lifetime of the vortex pair and rings, together with their fall velocity. The vortex ring lifetime can extend to 10 or more fall times. Tracer concentration distributions do not provide a reliable signature of the vortex dynamics, especially at later times after vortex linking. Aircraft properties, in particular the engine heat and placement, have a significant impact on the wake dynamics and appearance. We expect that the significant species fluctuations present during the vortex breakup period can affect important chemical reactions during this period.

When the mean atmospheric shear is sufficiently large that the product of the shear times the initial vortex-pair fall time is $O(1)$, the ambient vorticity can erode one member of the vortex pair, leading to a shorter mode breakup. We plan to explore more fully the effects of varying atmospheric conditions in future work as well as implementing some chemistry in the wake.

Acknowledgments

This work was supported by NASA Langley Research Center under Grant NAG 1 1635 with W. L. Grose as Technical Monitor. Initial conditions for the different aircraft wakes were supplied by Continuum Dynamics, Inc. We also thank R. I. Sykes for assistance with code modifications, M. K. Lewellen for taking the photographs used here, and C. W. Lewellen for help with the figures. Some results from the simulations considered here were originally presented at the NASA Atmospheric Effects of Aviation Project Annual Meeting, April 23–28, 1995.

References

[1]Hallock, J. N., "Aircraft Wake Vortices: An Annotated Bibliography (1923–1990)," U.S. Dept. of Transportation, DOT-FAA-RD-90-30, Cambridge, MA, Jan. 1991.

[2]Olsen, J., Goldberg, A., and Rogers, M. (eds.), *Aircraft Wake Turbulence and Its Detection*, Plenum, New York, 1971.

[3]Schumann, U., and Wurzel, D. (eds.), *Impact of Emissions from Aircraft and Spacecraft upon the Atmosphere*, Deutsche Forschungsanstalt für Luft- und Raumfahrt, DLR-Meiteillung 94-06, Cologne, Germany, 1994.

[4]Miake-Lye, R. C., Martinez-Shanchez, M., Brown, R. C., and Kolb, C. E., "Plume and Wake Dynamics, Mixing, and Chemistry Behind a High Speed Civil Transport Aircraft," *Journal of Aircraft*, Vol. 30, No. 4, 1993, pp. 467–479.

[5]Crow, S. C., "Stability Theory for a Pair of Trailing Vortices," *AIAA Journal*, Vol. 8, No. 12, 1970, pp. 2172–2179.

[6]Widnall, S. E., Bliss, D. B., and Zalay, A., "Theoretical and Experimental Study of the Stability of a Vortex Pair," *Aircraft Wake Turbulence and Its Detection*, edited by J. Olsen, A. Goldberg, and M. Rogers, Plenum, New York, 1971, pp. 305–338.

[7]Widnall, S. E., "The Structure and Dynamics of Vortex Filaments," *Annual Reviews of Fluid Mechanics*, Vol. 7, 1975, pp. 141–165.

[8]Crow, S. C., and Bate, E. R., Jr., "Lifespan of Trailing Vortices in a Turbulent Atmosphere," *Journal of Aircraft*, Vol. 13, No. 7, 1976, pp. 476–482.

[9]Bliss, D. B., "Effect of Unsteady Forcing on the Sinusoidal Instability of Vortex Wakes," *Journal of Aircraft*, Vol. 19, No. 9, 1982, pp. 713–721.

[10]Bilanin, A. J., Teske, M. E., and Williamson, G. G., "Vortex Interactions and Decay in Aircraft Wakes," *AIAA Journal*, Vol. 15, No. 2, 1977, pp. 250–260.

[11]Hill, F. M., "A Numerical Study of the Descent of a Vortex Pair in a Stably Stratified Atmosphere," *Journal of Fluid Mechanics*, Vol. 71, Pt. 1, 1975, pp. 1–13.

[12]Robins, R. E., and Delsi, D. P., "Numerical Study of Vertical Shear and Stratification Effects on the Evolution of a Vortex Pair," *AIAA Journal*, Vol. 28, No. 4, 1990, pp. 661–669.

[13]Boin, M., and Levkov, L., "Numerical Simulation of the Life Time of Contrails," *Impact of Emissions from Aircraft and Spacecraft upon the Atmosphere*, edited by U. Schumann and D. Wurzel, Deutsche Forschungsanstalt für Luft- und Raumfahrt, DLR-Meiteillung 94-06, Cologne, Germany, 1994, pp. 430–435.

[14]Gerz, T., and Palma, J., "Influence of Atmospheric Turbulence on the Development of an Idealized Airplane Wake: Numerical Studies," *Impact of Emissions from Aircraft and Spacecraft upon the Atmosphere*, edited by U. Schumann and D. Wurzel, Deutsche Forschungsanstalt für Luft- und Raumfahrt, DLR-Meiteillung 94-06, Cologne, Germany, 1994, pp. 309–314.

[15]Gierens, K. M., "Numerical Simulations of Persistent Contrails," Institut fur Physik der Atmosphare Rept. 30, Deutsche Forschungsanstalt fur Luft-und Raumfahrt e.V. (DLR), Oberpfaffenhofen, Germany, March 1995.

[16]Sarpkaya, T., and Daly, J. J., "Effect of Ambient Turbulence on Trailing Vortices," *Journal of Aircraft*, Vol. 24, No. 6, 1987, pp. 399–404.

[17]Liu, H. T., "Effects of Ambient Turbulence on the Decay of a Trailing Vortex Wake," *Journal of Aircraft*, Vol. 29, No. 2, 1992, pp. 255–263.

[18]Tombach, I., "Observations of Atmospheric Effects on Vortex Wake Behavior," *Journal of Aircraft*, Vol. 10, No. 11, 1973, pp. 641–647.

[19]Scorer, R. S., and Davenport, L. J., "Contrails and Aircraft Downwash," *Journal of Fluid Mechanics*, Vol. 43, Pt. 3, 1970, pp. 451–464.

[20]Sykes, R. I., and Henn, D. S., "Large Eddy Simulation of Turbulent Sheared Convection," *Journal of the Atmospheric Sciences*, Vol. 46, No. 8, 1989, pp. 1106–1118.

[21]Sykes, R. I., Lewellen, W. S., and Henn, D. S., "Numerical Simulation of the Boundary Layer Eddy Structure During the Cold-Air Outbreak of GALE IOP-2," *Monthly Weather Review*, Vol. 118, No. 2, 1990, pp. 363–374.

[22]Sykes, R. I., Parker, S. F., Henn, D. S., and Lewellen, W. S., "Turbulent Mixing with Chemical Reaction in the Planetary Boundary Layer," *Journal of Applied Meteorology*, Vol. 33, No. 7, 1994, pp. 825–834.

[23]Lewellen, D. C., Lewellen, W. S., and Yoh, S., "Influence of Bowen Ratio on Boundary Layer Cloud Structure," *Journal of the Atmospheric Sciences*, Vol. 55, No. 1, 1996, pp. 176–187.

[24]Farnell, L., "Solution of Poisson Equations on a Nonuniform Grid," *Journal of Computational Physics*, Vol. 35, No. 3, 1980, pp. 408–425.

[25]Quackenbush, T. R., Teske, M. E., and Bilanin, A. J., "Computation of Wake/Exhaust Mixing Downstream of Advanced Transport Aircraft," AIAA Paper 93-2944, July 1993.

[26]Dhanak, M. R., and deBernadinis, B., "The Oscillation of an Elliptic Vortex Ring," *Journal of Fluid Mechanics*, Vol. 109, 1981, pp. 189–216.

[27]Costen, R. C., Davidson, R. E., and Rogers, G. T., "Wind-Tunnel Tests and Computer Simulations of Buoyant Wing-Tip Vortices," *Journal of Aircraft*, Vol. 13, No. 7, 1976, pp. 495–499.